Transition Slow-Down by Rydberg Interaction of Neutral Atoms and a Fast Controlled-NOT Quantum Gate

Xiao-Feng Shi

School of Physics and Optoelectronic Engineering, Xidian University, Xi'an 710071, China

(Received 11 May 2020; revised 19 October 2020; accepted 22 October 2020; published 23 November 2020)

Exploring controllable interactions lies at the heart of quantum science. Neutral Rydberg atoms provide a versatile route toward flexible interactions between single quanta. Previous efforts mainly focused on the excitation annihilation (EA) effect of the Rydberg blockade due to its robustness against interaction fluctuation. We study another effect of the Rydberg blockade, namely transition slow-down (TSD). In TSD, a ground-Rydberg cycling in one atom slows down a Rydberg-involved state transition of a nearby atom, which is in contrast to EA that annihilates a presumed state transition. TSD can lead to an accurate controlled-NOT (CNOT) gate with a submicrosecond duration of about $2\pi/\Omega+\epsilon$ by two pulses, where ϵ is a negligible transient time to implement a phase change in the pulse and Ω is the Rydberg Rabi frequency. The speedy and accurate TSD-based CNOT gate makes neutral atoms comparable (superior) to superconducting (ion-trap) systems.

DOI: 10.1103/PhysRevApplied.14.054058

I. INTRODUCTION

There have recently been exciting advances in Rydberg atom quantum science [1–8] because of the feasibility to coherently and rapidly switch on and off the strong dipole-dipole interaction. Such interaction enables simulation of quantum many-body physics [9–22], probing and manipulation of single photons [23–35], large-scale entanglement generation [36,37], and quantum computation [36–50]. To date, however, most effort has focused on the effect of excitation annihilation (EA) proposed in Refs. [1,2] and reviewed in Refs. [3–8], although there are other categories as summarized in Table I. Belonging to the Rydberg blockade regime, EA involves single-atom Rydberg excitation and hence is not sensitive to the fluctuation of interactions. Besides EA, one can also excite both qubits to Rydberg states [1], or explore the antiblockade regime [51,52], or use the resonant dipole-dipole flip [11,35]. These latter processes, however, involve two-atom Rydberg excitation and are sensitive to the fluctuation of qubit separation that can substantially reduce the fidelity of a quantum control by using them [50]. It is an open question whether there is another means other than EA to explore the Rydberg blockade regime for efficient and high-fidelity quantum control.

Here, we study an unexplored transition slow-down (TSD) effect of the dipole-dipole interaction between Rydberg atoms. When the state of one atom oscillates back and forth between ground and Rydberg states, its Rydberg interaction does not block a Rydberg-involved state swap in a nearby atom, but slows it down, and the fold of slow-down is adjustable. The resulting TSD denotes the slow-down of the state transfer of one of the two atoms, although the collective Rabi frequency is enhanced due to the many-body effect. Though appearing as a slow-down, a controlled TSD on the contrary can drastically speed up certain crucial elements in a quantum computing circuit, such as the controlled-NOT (CNOT) gate that is the very important two-qubit entangling gate in the circuit model of quantum computing in both theory [53–58] and experiment [59,60]. TSD is an alternative route toward efficient, flexible, and high-fidelity quantum control over neutral atoms because it is implemented in the strong blockade regime that is robust to the fluctuation of interactions.

Though Rydberg atoms have kindled the flame for the ambition to large-scale quantum computing [1–5], and recent experiments demonstrate remarkable advances [38–50], further progress toward neutral-atom quantum computing is hindered by the difficulty to prepare a fast and accurate CNOT gate. This is partly because each of these CNOT gates was realized via combining an EA-based controlled-Z (C_Z) and a series of single-qubit gates [39–44], leading to CNOT gate durations dominated by single-qubit operations (e.g., over 4 μs in Refs. [43,44]). In contrast, a TSD-based CNOT gate has a duration of about $2\pi/\Omega+\epsilon$ by only two Rydberg pulses, i.e., needs no single-qubit rotations, where ϵ is a transient moment to implement a phase change in the pulses and Ω is the Rydberg Rabi frequency. Using the values of Ω and ϵ from Refs. [43,44], the TSD-based CNOT gate (duration approximately 0.3 μs) would be orders of magnitude faster

TABLE I. Summary of quantum science and technology based on two-body Rydberg interaction of neutral atoms (references are not complete but representative). There are in general two categories, the strong blockade regime and the frozen interaction regime, where the former was widely studied because of its robustness to fluctuation of interactions.

	Category	Blockade ($V \gg \Omega$)		Frozen interaction		
	Feature	Robust to fluctuation of V		Sensitive to fluctuation of V		
	Type of V	Dipole-dipole; Van der Waals		Van der Waals		Dipole-dipole
	Application	TSD	Excitation annihilation	Phase shift	Antiblockade	State flip
	Theoretical proposal	Here	Refs. [1,2]	Ref. [1]	Ref. [51]	(Intrinsic)
Realized	CNOT; Toffoli		Refs. [39–49]; Ref. [43]			
	Entanglement		Refs. [36–48]; for photons: Ref. [49]	Ref. [50]		
	Many-body; Optics		Refs. [12–22]; Refs. [23–33,35]		Refs. [51,52]	Refs. [9–11]; Ref. [35]

than those in Refs. [43,44], which means that a neutral-atom CNOT gate can be much faster than the CNOT gate (or ground Bell-state gate) by trapped ions [61–65] (note that the fast ion-trap gates in Refs. [66,67] are phase gates). Although still inferior to superconducting circuits [68,69] where CNOT gate times can be around 50 ns [70], the TSD-based CNOT gate is applicable in scalable neutral-atom platforms that are ideal for long-lived storage of quantum information at room temperatures.

II. A TWO-STATE CASE

The simplest model of TSD consists of two nearby atoms, each pumped by a laser pulse that induces a transition between a ground state $|1\rangle$ and a Rydberg state $|r\rangle$. The Rabi frequency is $\Omega_{c(t)}$ for the control (target) qubit, and the dipole-dipole interaction V in $|rr\rangle$ is assumed large compared to $\Omega_{c(t)}$ so that $|rr\rangle$ is not populated. For Rydberg interaction of the van der Waals type, V is limited because in this regime the native dipole-dipole interaction should be much smaller than the energy gaps between nearby two-atom Rydberg states [71], and thus the qubit spacing should be large enough. On the other hand, a direct dipole-dipole interaction can be huge for high-lying Rydberg states, although it is no longer a pure energy shift. In this sense, the residual blockade error of the order of approximately $\Omega_{c(t)}^2/V^2$ [72] can be negligible in the strong dipole-dipole interaction regime as long as the two-atom spacing is beyond the Le Roy radius.

In Fig. 1 we show a contrast between EA and a two-state TSD, where the pulse sent to the control atom is applied during $t \in [t_0, t_0 + t_1)$ and the pulse sent to the target atom is applied during $t \in [0, 2t_1)$ with $t_0 < t_1 \equiv \pi/\Omega_t$. Starting from an initial two-atom state $|11\rangle$, the wave function at $t = t_0$ becomes

$$|\psi(t_0)\rangle = \cos(\Omega_t t_0/2)|11\rangle - i\sin(\Omega_t t_0/2)|1r\rangle. \quad (1)$$

During $t \in [t_0, t_0 + t_1)$, the system Hamiltonian is

$$\hat{H} = [(\Omega_c|r1\rangle + \Omega_t|1r\rangle)\langle 11|/2 + \text{H.c.}] + \hat{H}', \quad (2)$$

where $\hat{H}'$ includes excitation between $\{|1r\rangle, |r1\rangle\}$ and $|rr\rangle$ and the dipole-dipole flip from $|rr\rangle$. Focusing on the strong interaction regime, $\hat{H}'$ can be discarded because $|rr\rangle$ is not

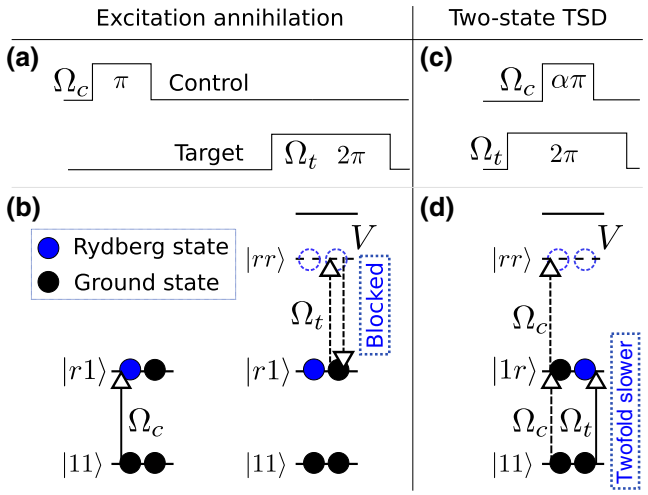

FIG. 1. Comparison between EA and TSD in two states. Black and blue circles represent ground and Rydberg states, respectively. Open circles denote Rydberg states not populated. (a) The first and second pulses in EA are sent to the control and target qubits, respectively, both for the transition between a ground state $|1\rangle$ and a Rydberg state $|r\rangle$. (b) State evolution starting from the two-qubit state $|11\rangle$ in EA. The blockade effect occurs in the second pulse, where the transition $|r1\rangle \leftrightarrow |rr\rangle$ is annihilated when $\Omega_t \ll V$. (c) In a two-state TSD, one pulse is applied to the target qubit with duration $2t_\pi$, within which another pulse is applied to the control qubit with duration t_π, where $t_\pi = \pi/\Omega_t$. The delay between the pulses for the two qubits is smaller than t_π. (d) The parameter $\alpha \equiv \Omega_c/\Omega_t$ depends on the desired extent of the TSD. With $\alpha = \sqrt{15}$, the Rydberg pumping of the target qubit, $|11\rangle \to |1r\rangle$, requires a 2π pulse, i.e., twice that when the control qubit is not pumped.

coupled [1] and, hence, $\hat{H} = \bar{\Omega}|\mathbb{R}\rangle\langle 11|/2 + \text{H.c.}$, where $\bar{\Omega} \equiv \sqrt{\Omega_c^2 + \Omega_t^2}$ and $|\mathbb{R}\rangle \equiv (\Omega_c|r1\rangle + \Omega_t|1r\rangle)/\bar{\Omega}$. When $\alpha \equiv \Omega_c/\Omega_t = \sqrt{15}$, we have $\bar{\Omega}t_1 = 4\pi$, so that the wave function at $t = t_0 + t_1$, given by $e^{-it_1\hat{H}}|\psi(t_0)\rangle$, is equal to Eq. (1), and it is like that nothing happens to the target qubit upon the completion of the drive in the control qubit. Then, because the pulse for the control qubit ends at $t = t_0 + t_1$, the continuous pumping of the target qubit drives the state to $|1r\rangle$ at $t = 2t_1$, i.e., a 2π pulse, instead of a π pulse, completes the transition $|11\rangle \to |1r\rangle$, which corresponds to a twofold slow-down.

III. A FAST CNOT GATE

To show the strength of TSD in quantum information, we consider TSD in three states. This is because the two-state TSD ends up in a Rydberg state that is not stable, while quantum information will be encoded with two qubit states $|0\rangle$ and $|1\rangle$ in the more stable ground manifold. For frequently used rubidium and cesium atoms, $|0\rangle$ and $|1\rangle$ can be chosen from the two hyperfine-split ground levels with a frequency difference of several gigahertz.

Consider a ground-Rydberg-ground transition chain $|0\rangle \leftrightarrow |r\rangle \leftrightarrow |1\rangle$, i.e., a state swap between the two long-lived qubit states via a metastable Rydberg state $|r\rangle$. The three-state TSD is implemented by pumping the control and target qubits with respective Rabi frequencies Ω_c and Ω_t for the same duration, with transition $|1\rangle \overset{\Omega_c}{\leftrightarrow} |r\rangle$ for the control qubit and $|0\rangle \overset{\Omega_t}{\leftrightarrow} |r\rangle \overset{\Omega_t}{\leftrightarrow} |1\rangle$ for the target qubit. This requires a setup capable of pumping both qubit states to a common Rydberg state in the target qubit, which is feasible, as experimentally demonstrated for two-atom entanglement about a decade ago [38] and for W-state preparation in atom ensembles later [36]. Because $|0\rangle$ is not pumped in the control qubit, the Hamiltonian is $\hat{\mathcal{H}}_{c0}(\Omega_t) = \Omega_t(|00\rangle + |01\rangle)\langle 0r|/2 + \text{H.c.}$ for the input states $|00\rangle$ and $|01\rangle$, where a subscript $c0$ ($c1$) denotes that the Hamiltonian applies when the input state for the control qubit is $|0(1)\rangle$. For the remaining input states, we consider the ordered basis $\{|1r\rangle, |r1\rangle, |r0\rangle, |11\rangle, |10\rangle\}$ for the Hamiltonian

$$\hat{\mathcal{H}}_{c1}(\Omega_c, \Omega_t) = \frac{1}{2}\begin{pmatrix} 0 & 0 & 0 & \Omega_t & \Omega_t \\ 0 & 0 & 0 & \Omega_c & 0 \\ 0 & 0 & 0 & 0 & \Omega_c \\ \Omega_t & \Omega_c & 0 & 0 & 0 \\ \Omega_t & 0 & \Omega_c & 0 & 0 \end{pmatrix}, \tag{3}$$

where we ignore the two-atom Rydberg state $|rr\rangle$ for the reasons given below Eq. (2). By diagonalizing Eq. (3) we have

$$\begin{aligned} |10\rangle &= \tfrac{1}{2}(|\mathscr{R}_4\rangle - |\mathscr{R}_3\rangle + |\mathscr{R}_2\rangle - |\mathscr{R}_1\rangle), \\ |11\rangle &= \tfrac{1}{2}(|\mathscr{R}_4\rangle - |\mathscr{R}_3\rangle - |\mathscr{R}_2\rangle + |\mathscr{R}_1\rangle), \end{aligned} \tag{4}$$

where $|\mathscr{R}_k\rangle$, $k = 1, \ldots, 4$, are four eigenvectors of Eq. (3), with eigenvalues $(\Omega_c, -\Omega_c, \overline{\Omega}, -\overline{\Omega})/2$, respectively [the fifth eigenvector does not enter Eq. (4)], where $\overline{\Omega} \equiv \sqrt{\Omega_c^2 + 2\Omega_t^2}$ and

$$\begin{aligned} |\mathscr{R}_{1,2}\rangle &= \tfrac{1}{2}[|r1\rangle - |r0\rangle \pm (|11\rangle - |10\rangle)], \\ |\mathscr{R}_{3,4}\rangle &= \frac{1}{2\overline{\Omega}}[\Omega_c(|r1\rangle + |r0\rangle) \pm \overline{\Omega}(|11\rangle + |10\rangle) + 2\Omega_t|1r\rangle]. \end{aligned} \tag{5}$$

We proceed to describe an accurate and exceedingly fast CNOT gate by a spin-echo assisted TSD. The sequence consists of two pulses, each with duration π/Ω_c and condition $|\Omega_t|/\Omega_c = \sqrt{6}/2$, shown in Fig. 2(a). A π phase change (requiring a time ϵ) is inserted between the pulses sent to the target qubit so as to induce spin echo, where ϵ can be around 10 ns [43]. The spin echo suppresses the state swap of the target qubit if the control qubit is initialized in $|0\rangle$ [73,74]; when the control qubit is initialized in $|1\rangle$, it is pumped to $|r\rangle$, resulting in TSD in the target qubit. Then, the transition $|0\rangle \rightleftharpoons |r\rangle \rightleftharpoons |1\rangle$ in the target qubit, which can occur within a pulse duration of $\sqrt{2}\pi/\Omega_t$ if no TSD is used [75], can still occur with a $\sqrt{3}$-fold slow-down. The mechanism is understood in two steps. First, during $t \in [0, t_\pi)$ with $t_\pi = \pi/\Omega_c$, the input state $|\psi_{c0}(0)\rangle = |00\rangle$ or $|01\rangle$ evolves according to $e^{-it\mathcal{H}_{c0}(\Omega_t)}|\psi_{c0}\rangle$, and after a π phase change to the Rydberg Rabi frequency that may require a finite transient time ϵ, the state evolution becomes $e^{-i(t-t_\pi-\epsilon)\mathcal{H}_{c0}(-\Omega_t)}|\psi_{c0}(t_\pi)\rangle$ during the second pulse, leading to $e^{-it\mathcal{H}_{c0}(-\Omega_t)t_\pi}|\psi_{c0}(t_\pi)\rangle = e^{-it\mathcal{H}_{c0}(-\Omega_t)t_\pi}e^{-it\mathcal{H}_{c0}(\Omega_t)t_\pi}|\psi_{c0}(0)\rangle = |\psi_{c0}(0)\rangle$ at the end of the sequence. Second, according to Eq. (5), the first pulse during $t \in [0, t_\pi)$ evolves the input state $|\psi_{c1}(0)\rangle = |10\rangle$ according to

$$\tfrac{1}{2}(e^{it\overline{\Omega}/2}|\mathscr{R}_4\rangle - e^{-it\overline{\Omega}/2}|\mathscr{R}_3\rangle + e^{it\Omega_c/2}|\mathscr{R}_2\rangle - e^{-it\Omega_c/2}|\mathscr{R}_1\rangle), \tag{6}$$

which becomes

$$|\psi_{c1}(t_\pi)\rangle = \tfrac{1}{2}(i|\mathscr{R}_1\rangle + i|\mathscr{R}_2\rangle + |\mathscr{R}_3\rangle - |\mathscr{R}_4\rangle) \tag{7}$$

at $t = t_\pi$ because $(t_\pi\Omega_c, t_\pi\overline{\Omega}) = (\pi, 2\pi)$. In Eq. (7), the eigenvectors $|\mathscr{R}_j\rangle$, $j = 1, \ldots, 4$, are defined in Eq. (5) with Rabi frequencies (Ω_c, Ω_t) during $t \in [0, t_\pi)$. During $t \in t_\pi + \epsilon + [0, t_\pi)$, the Hamiltonian has Rabi frequencies $(\Omega_c, -\Omega_t)$ with the eigenvectors $|\mathscr{R}_{1,2}\rangle$ the same as in Eq. (5), but the expressions for $|\mathscr{R}_{3,4}\rangle$ become

$$|\mathscr{R}'_{3,4}\rangle = \frac{1}{2\overline{\Omega}}[\Omega_c(|r1\rangle + |r0\rangle) \pm \overline{\Omega}(|11\rangle + |10\rangle) - 2\Omega_t|1r\rangle]. \tag{8}$$

Using Eqs. (5) and (8), Eq. (7) becomes

$$|\psi_{c1}(t_\pi)\rangle = e^{-it_\pi \mathcal{H}_{c1}(\Omega_c,-\Omega_t)}|\psi_{c1}(0)\rangle, \tag{9}$$

i.e., the state at $t = t_\pi$ is as if Rabi frequencies $(\Omega_c, -\Omega_t)$ were used during the first pulse. Equation (9) is the key feature enabling a fast CNOT gate. After the second pulse, the state at $t = 2t_\pi + \epsilon$ becomes $e^{-it_\pi \mathcal{H}_{c1}(\Omega_c,-\Omega_t)}|\psi_{c1}(t_\pi)\rangle$ that can be rewritten as $e^{-2it_\pi \mathcal{H}_{c1}(\Omega_c,-\Omega_t)}|\psi_{c1}(0)\rangle$ thanks to Eq. (9), which further reduces to $|11\rangle$ according to Eqs. (4) and (6). A similar analysis shows that if the initial state is $|11\rangle$, it maps to $|10\rangle$ upon the completion of the pulse. So we realize the map

$$\{|00\rangle, |01\rangle, |10\rangle, |11\rangle\} \to \{|00\rangle, |01\rangle, |11\rangle, |10\rangle\}, \tag{10}$$

which is the standard CNOT gate. A numerical simulation of the population evolution by $\mathcal{H}_{c0}$ and $\mathcal{H}_{c1}$ in Eq. (3) is shown in Figs. 2(c) and 2(d) for the input states $|00\rangle$ and $|10\rangle$, respectively, where the transient time ϵ is ignored for brevity.

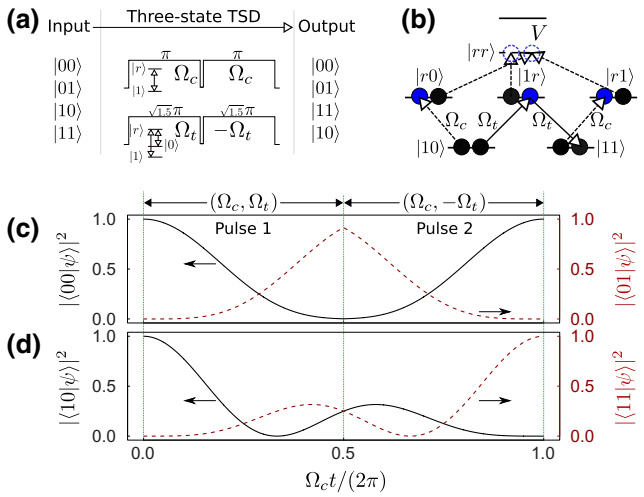

FIG. 2. A three-state TSD and a fast CNOT gate by two pulses. (a) A three-state TSD is realized by sending two pulses with equal duration π/Ω_c to each qubit. The Rabi frequencies are Ω_c (Ω_c) and Ω_t $(-\Omega_t)$ for the control and target qubits in the first (second) pulse, where $\Omega_t = \sqrt{1.5}\Omega_c$. (b) Relevant transitions for $|10\rangle \to |11\rangle$. Transitions involving $|00\rangle$ and $|01\rangle$ are not shown because they do not involve dipole-dipole interaction. The left or right pointing arrows are intended to clarify the protocol, not denote a change in angular momentum. (c) The input state $|00\rangle$ transitions back to itself because of the spin echo by $\Omega_t \to -\Omega_t$. (d) With the same pumping, the input state $|10\rangle$ transitions to $|11\rangle$ at the end of the pulse sequence. The time for implementing the phase change between the two pulses is not shown for brevity (see the text). The duration of the two pulses is $2\pi/\Omega_c = \sqrt{6}\pi/\Omega_t$, corresponding to a $\sqrt{3}$-fold slow-down because the state swap $|0\rangle \to |r\rangle \to |1\rangle$ in the target qubit can occur within a pulse duration of $\sqrt{2}\pi/\Omega_t$ if no TSD is used.

High fidelity is possible with the TSD-based CNOT gate. To estimate the intrinsic fidelity limited by Rydberg-state decay and Doppler dephasing, we considered atomic levels and Rydberg laser Rabi frequencies in recent experiments [43,44], and numerically found that the fidelity of the TSD-based CNOT gate or Bell state would reach 99.9% (99.8%) with experimentally affordable effective temperatures $T_a = 5$ (15) μK of qubit motion [42,44,48]. As detailed in Appendix A 2, this estimate assumes that the fields for $|0\rangle \to |r\rangle$ and $|1\rangle \to |r\rangle$ in the target qubit copropagate, leading to opposite phases in the two transitions of the chain $|0\rangle \xrightarrow{\Omega_t e^{itkv_t}} |r\rangle \xrightarrow{\Omega_t e^{-itkv_t}} |1\rangle$, where k is the wavevector and v_t is the speed of the target qubit along the propagation direction of light. Then, the state transfer from $|0\rangle$ to $|1\rangle$ (or the reverse) picks up two opposite phases $\pm tkv_t$ that partly suppress the dephasing. Fortunately, our method is not strictly dependent on the above dephasing-resilient configuration. For example, for the worst case of counterpropagating fields such that the sequential state transfer from $|0\rangle$ to $|1\rangle$ picks up a total phase $2tkv_t$, the simulation in Appendix A shows that fidelity over 99.6% is achievable for $T_a \sim 15$ μK at room temperatures. The robustness against Doppler dephasing benefits from the avoidance of shelving the control atom on the Rydberg level in free flight during pumping of the target atom, as required in an EA-based CNOT gate [75,76].

The above analysis assumes that $V/2\pi = 500$ MHz, corresponding to an interatomic distance $l = 3$ μm. When $V/2\pi = 100$ MHz with larger $l = 4.6$ μm (where crosstalk can be negligible [44]), the fidelity would be 99.8% (99.7%) with $T_a = 5$ (15) μK at room temperatures (see Appendix B for details). This benefits from the fact that our CNOT gate is not sensitive to the change of interaction V in the strong blockade regime. Finally, with fluctuation (of relative Gaussian width σ) of the two Rabi frequencies for the two transitions $|0(1)\rangle \leftrightarrow |r\rangle$ in the target qubit, a very small extra error in the range $(0.02, 0.4)\%$ arises for σ in the range $(1, 5)\%$ as detailed in Appendix C. So, high fidelity is achievable since the power fluctuation of Rydberg lasers can be well suppressed [43,47].

IV. DISCUSSION AND CONCLUSIONS

The CNOT gate in Eq. (10) is implemented within a short time $2\pi/\Omega_c = \sqrt{6}\pi/\Omega_t$ plus a transient moment ϵ for a phase change between the two pulses, where ϵ can be negligible as in Ref. [43]. Although a phase twist is used in both Ref. [43] and here, our TSD method is drastically different in physics from the method of Ref. [43], as discussed in Appendix D. Note that Eq. (10) does not depend on any single-qubit gates if one starts from Eq. (3). If s- or d-orbital Rydberg states are used, two-photon transitions can be applied that lead to ac Stark shifts for the ground and Rydberg states. As shown in Appendix E, these shifts

are annulled in Eq. (3), which is achievable by choosing an appropriate ratio between the detuning at the intermediate state and the magnitudes of the fields for the lower and upper transitions [41].

Our CNOT gate duration can be less than 0.3 μs with Rydberg Rabi frequencies [$2\pi \times (3.5 \sim 4.6)$ MHz] like those realized in Refs. [43,44] that showed CNOT gate durations orders of magnitude longer than here. Previous CNOT gates [39–44] required two or more single-qubit rotations to convert C_Z to a CNOT gate, which was usually achieved with two-frequency Raman light [39,40,42,43], or with microwave driving assisted by the Stark shift of laser fields [41,44]. High-fidelity realizations of such gates came with long gate durations [43,44,77,78], although they can also be carried out rapidly in proof-of-principle experiments [79,80] where high fidelity is not concerned. The atom traps have finite lifetimes [4] and a faster protocol can lead to more CNOT cycles before the qubit arrays should be reloaded. Because a practical quantum processor tackling real problems uses a series of quantum gates including CNOT gates [53–60], certain computational tasks can be executed only with fast enough CNOT gates in each cycle of laser cooling and loading of the atom array. The studied speedup of the minimal functional quantum circuit shows a possible way to address the problem of finite lifetime of atom traps that limits the capability of a neutral-atom quantum processor. Moreover, concerning the ratio between the coherence time and the CNOT gate time, the TSD method makes neutral-atom systems competitive with superconducting and ion-trap systems, as compared in detail in Appendix F.

In conclusion, we explore another effect of Rydberg blockade by dipole-dipole interaction in neutral atoms, namely the effect of TSD. We show that TSD can speed up a neutral-atom quantum computer by proposing an exceedingly fast TSD-based CNOT gate realized by two pulses separated by a short transient moment for changing the phase of the pulse. The exotic TSD is an excellent effect of dipole-dipole interactions other than the well-known excitation annihilation effect that can push Rydberg-atom quantum science to another level.

ACKNOWLEDGMENTS

The author thanks Yan Lu for useful discussions. This work is supported by the National Natural Science Foundation of China under Grant No. 11805146 and the Natural Science Basic Research plan in Shaanxi Province of China under Grant No. 2020JM-189.

APPENDIX A: GATE FIDELITY

Before analyzing the gate error, we emphasize that TSD is particularly useful for speeding up the minimal functional quantum circuit, namely the CNOT gate. The CNOT protocols by EA in previous methods involve multiple switchings of the external control fields that bring extra complexity to the experimental implementation, elongate the gate duration, and introduce extra errors from the fluctuation of the control fields and from the intrinsic atomic Doppler broadening. Previous effort for suppressing these errors includes a C_Z gate based on quantum interference [43,81], but going from C_Z to the more useful CNOT gate (or to create Bell states in the ground-state manifold) still needs several single-qubit operations [39–44]. For example, the first experimental neutral-atom CNOT gate needed five or seven pulses [39], and the CNOT gate in Ref. [43] used two (four) pulses in the control (target) qubit besides several short pulses for phase compensation. The central procedure of the CNOT gate in Ref. [43] is via combining (i) a two-qubit C_Z-like gate by two pulses of duration about $2.7\pi/\Omega$ with a phase change inserted between the pulses that requires an extra transient time ϵ, (ii) a short pulse to compensate an intrinsic phase to recover a C_Z from the C_Z-like gate, and (iii) two single-qubit rotations of duration $\pi/\Omega_{\rm hf}$ (approximately 2 μs therein) in the target qubit, where Ω is the Rydberg laser Rabi frequency and $\Omega_{\rm hf}$ is the hyperfine laser Rabi frequency between the two qubit states. Page 4 of Ref. [43] indicates that the C_Z-like gate needs 0.4 μs, and it had $(\Omega_{\rm hf}, \Omega)/(2\pi) = (0.25, 3.5)$ MHz (see pp. 1 and 2 of Ref. [43]), and, thus, $\epsilon = 0.4\ \mu{\rm s} - 2.732\pi/\Omega \approx 9.7$ ns; we assume such a fast phase change time here. Figure 3(d) of Ref. [43] presents a CNOT sequence with durations equal to those of two $X(\pi/2)$, one $X(\pi)$, and the C_Z-like gate, i.e., $2\times\pi/(2\Omega_{\rm hf}) + \pi/\Omega_{\rm hf} + 2.7\pi/\Omega$, and thus the CNOT sequence needs about 4.4 μs therein (the actual gate durations should be larger when accounting for gaps between pulses therein). In contrast, the TSD-based CNOT sequence needs a duration of about $\sqrt{6}\pi/\Omega_t$, which is only 0.27 (0.35) μs with $\Omega_t/(2\pi) =$ 4.6 (3.5) MHz from Ref. [44] (Ref. [43]).

One may assume that if the single-qubit rotations in Refs. [43,44] are implemented by the transition chain $|0\rangle \leftrightarrow |r\rangle \leftrightarrow |1\rangle$, their gate durations will also be small. But there is a problem with this assumption, due to the fact that the single-qubit rotations necessary to transform a C_z gate to a CNOT gate are two $X(\pi/2)$ gates that transfer $\{|0\rangle, |1\rangle\}$ to $\{|0\rangle - i|1\rangle, -i|0\rangle + |1\rangle\}/\sqrt{2}$ [see Fig. 5(a) of Ref. [44] or Fig. 3(d) of Ref. [43]]. The pumping by $\hat{\mathbb{H}}(\Omega_t) = \Omega_t(|0\rangle + |1\rangle)\langle r|/2 + {\rm H.c.}$ cannot achieve this since one can easily prove that starting from $|\varphi\rangle = |0\rangle$, the populations in $\{|0\rangle, |r\rangle, |1\rangle\}$ will be $\frac{1}{2}\{2\cos^4\theta/2, \sin^2\theta, 2\sin^4\theta/2\}$, where $\theta = t\Omega_t/\sqrt{2}$. This means that there is no way to use the resonant transition chain $|0\rangle \leftrightarrow |r\rangle \leftrightarrow |1\rangle$ for the $X(\pi/2)$ rotation. On the other hand, one may also assume that a succession of a π pulse on $|1\rangle \to |r\rangle$, a $\pi/2$ pulse on $|r\rangle \to |0\rangle$, and a π pulse on $|r\rangle \to |1\rangle$ can, e.g., realize a $X(\pi/2)$ rotation. However, the extra time to shelve an atom in a Rydberg state leads to extra Doppler dephasing, and the frequent turning on and off of Rydberg lasers can lead to extra atom loss [41].

Below, we analyze gate imperfections due to the prevailing intrinsic Rydberg-state decay and Doppler broadening. These are the dominant intrinsic errors in gate operations [44], while technical issues such as laser noise are in principle not fundamental. From here to Appendix C, we take, as an example, ^{87}Rb qubits and consider the intermediate level $6P_{3/2}$ for Rydberg pumping, where the two detunings at $6P_{3/2}$ should be different for the two transitions $|0\rangle \overset{\Omega_t}{\longleftrightarrow} |r\rangle$ and $|1\rangle \overset{\Omega_t}{\longleftrightarrow} |r\rangle$. For an s-orbital rubidium Rydberg state with principal quantum number around 70, the lifetime of $|r\rangle$ is about $\tau = 400$ (150) μs at a temperature of 4 (300) K by the estimate in Ref. [82]. When the lower and upper fields counterpropagate along, e.g., **z**, the wavevector is $k = 2\pi(1/420.3 - 1/1012.7)$ nm^{-1} [83]. We assume that the two qubits are initially located at the centers of the traps at $(0, 0, x_0)$ and $(0, 0, 0)$, respectively. The traps are usually turned off during Rydberg pumping, and the free flight of the qubits leads to time-dependent Rabi frequencies $\Omega_c e^{it(kv_c+x_0)}$ for the control qubit, and $(\Omega_t e^{itkv_t}, \Omega_t e^{itkv_t})$ for the two transitions $|0(1)\rangle \leftrightarrow |r\rangle$ in the target qubit, where (v_c, v_t) are the projections of velocity along **z** for the control and target qubits, respectively. With a finite atomic temperature T_a, there is a finite distribution $\mathscr{D}(v_c)\mathscr{D}(v_t)$ for the speeds (v_c, v_t), where $\mathscr{D}(v)$ is a Gaussian [44,83].

1. Rydberg-state decay

Although the gate duration, when neglecting the transient time (less than 10 ns, as shown above) for the phase change in the pulses, is $t_g = 2\pi/\Omega_c$, the main decay error arises when the atoms are in a Rydberg state [72], supposing the intermediate state is largely detuned. By using the estimate in Ref. [84], the decay error of the TSD-based CNOT gate can be approximated as

$$E_{\rm decay} = \frac{1}{4\tau}\int dt\Big\{\sum_{|\psi(0)\rangle=|00\rangle,|01\rangle} |\langle 0r|\psi(t)\rangle|^2 + \sum_{|\psi(0)\rangle=|10\rangle,|11\rangle} [|\langle r0|\psi(t)\rangle|^2 + |\langle r1|\psi(t)\rangle|^2 + |\langle 1r|\psi(t)\rangle|^2]\Big\}, \quad \text{(A1)}$$

which is $0.39t_g$ by numerical simulation. Consider a set of experimentally feasible [44] values of Rydberg Rabi frequencies $\Omega_c = \Omega_t/\sqrt{1.5} = 2\pi \times 3.6$ MHz; we have $E_{\rm decay} = 2.7$ (7.2) $\times 10^{-4}$ for qubits in an environment temperature of 4 (300) K. Alternatively, a more detailed numerical simulation that uses the optical Bloch equation in the Lindblad form with correct branching ratios [81] can predict a slightly lower $E_{\rm decay}$ because some populations can decay to qubit states that will again contribute to the gate operation.

TABLE II. Rotation errors (scaled up by 10^4; excluding Rydberg-state decay) of the TSD-based CNOT gate by $\Omega_c/2\pi =$ 3.5 MHz for the cases where the propagation directions for the fields on the target qubit are switched between the first and second pulses (case 2) and where no such switching occurs (case 1). Here Eq. (A6) is used that accounts for the phase errors and the truth table errors.

	T (μK)	5	10	15	20	50
Case 1	$10^4 \times \overline{E_{\rm ro}}$	4.31	8.09	11.9	15.6	38.2
Case 2	$10^4 \times \overline{E_{\rm ro}}$	3.11	5.69	8.26	10.8	26.2

2. Doppler dephasing

For the TSD-based CNOT gate to be resilient to Doppler dephasing, the two fields for the lower transitions $|0\rangle \to |p\rangle$ and $|1\rangle \to |p\rangle$ copropagate along **z**, and those for their upper transitions $|p\rangle \to |r\rangle$ copropagate along $-$**z**, so that the wavevectors for $|0(1)\rangle \to |r\rangle$ have (approximately) the same value k. Here $|p\rangle$ is symbolic for the intermediate $6P_{3/2}$ state; note that the detunings at $|p\rangle$ for the two transition chains must have a large difference. Alternatively, we can use different fine states in the $6p$ manifold for the two transition chains (the numerical results in Tables II and III stay similar). Then, the transition $|0\rangle \overset{\Omega_t}{\to} |r\rangle \overset{\Omega_t}{\to} |1\rangle$ becomes

$$|0\rangle \xrightarrow{\Omega_t e^{itkv_t}} |r\rangle \xrightarrow{\Omega_t e^{-itkv_t}} |1\rangle \quad \text{(A2)}$$

when accounting for the atom drift. The above transition mainly transfers the population between the two hyperfine states, which means that if the negligible population stays at $|r\rangle$, the two phases tkv_t and $-tkv_t$ add up for any moment, leading to negligible phase noise because $tkv_t - tkv_t = 0$ for the population transfer from $|0\rangle$ to $|1\rangle$. However, this is not ideal since there is always some population at $|r\rangle$ during the process. Nonetheless, that there is partial phase cancellation can suppress the Doppler dephasing compared to usual cases.

For the control qubit, the transition $|1\rangle \xrightarrow{\Omega_c e^{itkv_c}} |r\rangle$ still has the usual Doppler dephasing. However, the pumping $|1\rangle \xrightarrow{\Omega_c e^{itkv_c}} |r\rangle$ in the control is immersed in the TSD and does not put much population in the Rydberg state. Numerical simulation shows that $\int dt[|\langle r0|\psi(t)\rangle|^2 +$

TABLE III. Fidelity errors (scaled up by 10^4; excluding Rydberg-state decay) of the Bell state by the TSD-based CNOT gate, with the same pulse sequence as used for Table II. Here an overbar denotes the ensemble average as in Eq. (A7).

	T (μK)	5	10	15	20	50
Case 1	$10^4 \times \overline{E_{\rm Bell}}$	2.86	5.27	7.67	10.1	24.4
Case 2	$10^4 \times \overline{E_{\rm Bell}}$	2.57	4.67	6.78	8.88	21.4

$|\langle r1|\psi(t)\rangle|^2] = 0.31t_g$ for either $|\psi(0)\rangle = |00\rangle$ or $|01\rangle$ in each gate sequence.

To show the robustness of the TSD-based CNOT gate against Doppler dephasing, we numerically simulate the state evolution by using $\hat{\mathcal{H}}_{c0}(\Omega_t e^{itkv_t}) = \Omega_t(e^{-itkv_t}|00\rangle + e^{-itkv_t}|01\rangle)\langle 0r|/2 + \text{H.c.}$ for the input states $|00\rangle$ and $|01\rangle$, and

$$\hat{\mathcal{H}}_{c1}(\Omega_c e^{itkv_c}, \Omega_t e^{itkv_t}) = \frac{1}{2}\begin{pmatrix} 2V & \Omega_c e^{itkv_c} & \Omega_t e^{itkv_t} & \Omega_t e^{itkv_t} & 0 & 0 \\ \Omega_c e^{-itkv_c} & 0 & 0 & 0 & \Omega_t e^{itkv_t} & \Omega_t e^{itkv_t} \\ \Omega_t e^{-itkv_t} & 0 & 0 & 0 & \Omega_c e^{itkv_c} & 0 \\ \Omega_t e^{-itkv_t} & 0 & 0 & 0 & 0 & \Omega_c e^{itkv_c} \\ 0 & \Omega_t e^{-itkv_t} & \Omega_c e^{-itkv_c} & 0 & 0 & 0 \\ 0 & \Omega_t e^{-itkv_t} & 0 & \Omega_c e^{-itkv_c} & 0 & 0 \end{pmatrix} \tag{A3}$$

for the input states $|10\rangle$ and $|11\rangle$, where Eq. (A3) is written with the basis $\{|rr\rangle, |1r\rangle, |r1\rangle, |r0\rangle, |11\rangle, |10\rangle\}$, where V represents the interaction of the state $|rr\rangle$. Because of Doppler dephasing, the gate map in the basis $\{|00\rangle, |01\rangle, |10\rangle, |11\rangle\}$ changes from the ideal form

$$U = \begin{pmatrix} 1 & 0 & 0 & 0 \\ 0 & 1 & 0 & 0 \\ 0 & 0 & 0 & 1 \\ 0 & 0 & 1 & 0 \end{pmatrix} \tag{A4}$$

to

$$\mathcal{U} = \begin{pmatrix} a & b & 0 & 0 \\ c & d & 0 & 0 \\ 0 & 0 & e & f \\ 0 & 0 & g & h \end{pmatrix}, \tag{A5}$$

where a, b, c, and d can be calculated by sequentially using $\hat{\mathcal{H}}_{c0}(\Omega_t)$ and $\hat{\mathcal{H}}_{c0}(-\Omega_t)$ for the input states $|00\rangle$ and $|01\rangle$, while e, f, g, and h can be calculated using, sequentially, $\hat{\mathcal{H}}_{c1}(\Omega_c, \Omega_t)$ and $\hat{\mathcal{H}}_{c1}(\Omega_c, -\Omega_t)$ for the input states $|10\rangle$ and $|11\rangle$. To study the robustness to Doppler dephasing, we would like to see errors mainly from the Doppler dephasing if the blockade error is negligible. So we adopt a large blockade interaction $V/(2\pi) = 500$ MHz as in Ref. [85]. We choose $\Omega_c = \Omega_t/\sqrt{1.5} = 2\pi \times 3.6$ MHz, define the rotation error as [86]

$$E_{\text{ro}} = 1 - \tfrac{1}{20}[|\text{Tr}(U^\dagger \mathcal{U})|^2 + \text{Tr}(U^\dagger \mathcal{U}\mathcal{U}^\dagger U)], \tag{A6}$$

and evaluate the ensemble average with

$$\overline{E_{\text{ro}}} \approx \frac{\sum_{v_c}\sum_{v_t} E_{\text{ro}}(v_c, v_t)\mathcal{D}(v_c)\mathcal{D}(v_t)}{\sum_{v_c}\sum_{v_t}\mathcal{D}(v_c)\mathcal{D}(v_t)}, \tag{A7}$$

where the sum is over 10^4 sets of speeds (v_c, v_t), where $v_{c(t)}$ applies 101 values equally distributed from -0.5 to 0.5 m/s because the atomic speed has little chance to be over 0.5 m/s for the temperatures $T_a \leq 50$ μK considered in this work. The approximation by Eq. (A7) is not much different from a rigorous integration. More details can be found in Ref. [83] for the method of numerical simulation.

Case 1. Using $\hat{\mathcal{H}}_{c0}(\Omega_t e^{itkv_t})$ (for $\{|00\rangle, |01\rangle\}$) and $\hat{\mathcal{H}}_{c1}(\Omega_c e^{itkv_c}, \Omega_t e^{itkv_t})$ (for $\{|10\rangle, |11\rangle\}$) for the first pulse, and $\hat{\mathcal{H}}_{c0}(\Omega_t e^{itkv_t})$ and $\hat{\mathcal{H}}_{c1}(\Omega_c e^{itkv_c}, -\Omega_t e^{itkv_t})$ for the second pulse, we give the ensemble-averaged rotation errors in Table II (see the case-1 row), with effective atomic temperatures above $T_a = 5$ μK that are achievable in experiments [48]. From these results, we see that the CNOT fidelity $1 - E_{\text{decay}} - \overline{E_{\text{ro}}}$ can reach 99.9% with qubits cooled to around $T_a = 10$ (5) μK in a 4 (300) K environment.

Case 2. To further suppress Doppler dephasing, we consider switching propagation directions of fields for the control qubit between the two pulses. In other words, the Hamiltonians (for $\{|00\rangle, |01\rangle\}$) are $\hat{\mathcal{H}}_{c0}(\Omega_t e^{itkv_t})$ and $\hat{\mathcal{H}}_{c0}(-\Omega_t e^{-itkv_t})$ for the first and second pulses, respectively. The ensemble-averaged rotation errors are given in Table II (see the case-2 row). From the results in Table II, we can see that the CNOT fidelity $1 - E_{\text{decay}} - \overline{E_{\text{ro}}}$ slightly improves if this latter configuration case is employed. The mechanism for the extra suppression of Doppler dephasing in this latter case stems from the fact that the population going, e.g., from $|0\rangle$ to $|1\rangle$, obtains some phase error due to the actions $\Omega_t e^{-it'kv_t}|1\rangle\langle r|$ and $\Omega_t e^{itkv_t}|r\rangle\langle 0|$; subsequently, the second pulse pumps $|1\rangle$ to $|0\rangle$ and induces some phase error due to the actions $-\Omega_t e^{-it'kv_t}|r\rangle\langle 1|$ and $-\Omega_t e^{itkv_t}|0\rangle\langle r|$, meaning that the phase terms between the two pulses are continuous, which is better for the desired transition to occur. For case 1, the pumping from $|0\rangle$ to $|r\rangle$ has a phase term tkv_t at the end of pulse 1, which becomes $-tkv_t$ when the population begins to go back at the start of pulse 2, i.e., there is a phase jump. More details about the influence on gate fidelity from atom-drift-induced phase change in Rabi frequencies can be found in Ref. [83].

Since this latter case is a little involved and the increase of fidelity is marginal, it is only of interest in the future when technical issues are resolved so that a fidelity level beyond 99% is technically achievable.

The result in Table II accounts for both the population errors and the phase errors. In experiments, the phase errors are not usually important, especially in the characterization of the Bell state [43,44]. Thus, we continue to study the strength of the TSD-based CNOT gate for achieving high-fidelity Bell states.

3. High-fidelity Bell states

A TSD-based CNOT operation can map the initial product state $|\psi(0)\rangle = (|00\rangle + |10\rangle)/\sqrt{2}$ to the Bell state $|\Phi\rangle = (|00\rangle + |11\rangle)/\sqrt{2}$ without resorting to extra single-qubit gates (except the state initialization). The Rydberg superposition time is equal to that in Appendix A 1. We follow Ref. [43] by evaluating the infidelity as $E_{\rm Bell} = 1 - \langle\Phi|\rho(t)|\Phi\rangle$, where $\rho(t) = |\psi\rangle\langle\psi|$ with $|\psi\rangle$ evolved by using the pulse sequence as in Appendix A 2 for the input state $|\psi(0)\rangle$. The numerical results are given in Table III, which show that at room temperatures the Bell state can be created with a fidelity of 99.88% if qubits are cooled to the level of $T_a = 10$ μK, which is affordable according to the atom cooling achieved in previous experiments [42,48].

Finally, we emphasize that it is not so crucial to have the Doppler-resilient configuration (with copropagating fields) for the two transition chains in the target qubit, as discussed around Eq. (A2). Consider the worst case with largest dephasing, i.e., if the two sets of fields counterpropagate so that Eq. (A2) becomes $|0\rangle \xrightarrow{\Omega_t e^{itkv_t}} |r\rangle \xrightarrow{\Omega_t e^{itkv_t}} |1\rangle$; then the motional dephasing error should be larger. For example, we numerically find that the Bell-state errors in the second row (case 1) of Table III become $(9.72\times10^{-4}, 1.90\times10^{-3}, 2.82\times10^{-3}, 3.74\times10^{-3}, 9.22\times10^{-3})$ for $T_a = (5, 10, 15, 20, 50)$ μK; similar results can be found for the TSD-based CNOT gate. With $E_{\rm decay} = 7.2\times10^{-4}$ for qubits in an environment of 300 K, the Bell-state fidelity would be 99.65% at $T_a = 15$ μK. This still large fidelity means that, for experimental convenience, high fidelity is possible with any configuration of propagation directions for the two sets of fields if errors other than the intrinsic Doppler dephasing and Rydberg-state decay can be avoided.

APPENDIX B: INTERATOMIC DISTANCES

The dipole-dipole interaction V is a function of interatomic distance $\mathcal{L}$. For V to be large enough so that the blockade error is negligible, $\mathcal{L}$ should be small enough. In order to avoid wave function overlap, the distance between the nuclei of the two Rydberg atoms is larger than the Le Roy distance that can be calculated using the

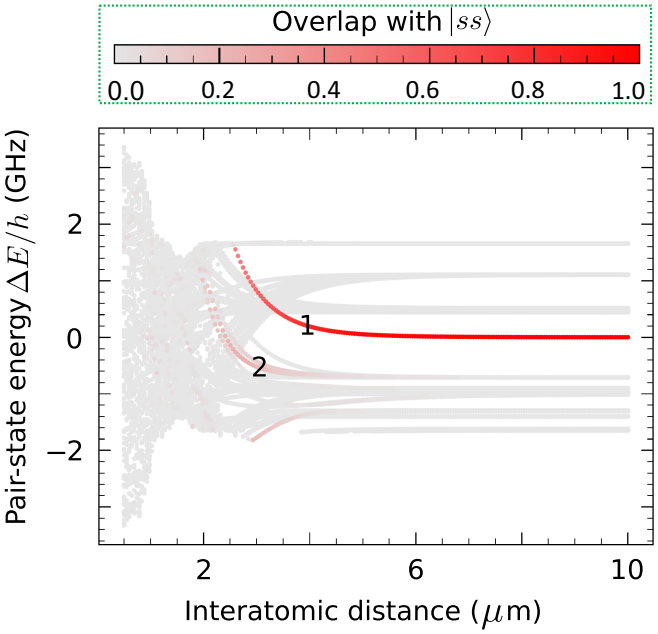

FIG. 3. Energy spectrum for two ^{87}Rb atoms lying along the quantization axis when initialized in the two-atom pair state $|ss\rangle \equiv |70S_{1/2}, m_J = 1/2; 70S_{1/2}, m_J = 1/2\rangle$ [87]. Here 1 and 2 label the two states that have largest overlap with $|ss\rangle$ and nearest to the unperturbed energy (labeled as zero).

open source library of Ref. [87]. For the parameters chosen as an example in this work, the Le Roy distance is 1.50 μm for two rubidium atoms in the state $70S_{1/2}$, and we can consider longer interatomic distances in the range $\mathcal{L} > 2.6$ μm. The dipole-dipole interaction will couple the two-atom state $|70S_{1/2}, m_J = \frac{1}{2}; 70S_{1/2}, m_J = \frac{1}{2}\rangle$ to many other states. To find the interaction, we consider states $|nL; n'L'\rangle$ coupled from the initial states (n and L denote the principal and angular momentum quantum numbers, respectively), with $|n - 70|, |n' - 70| \le 5$, and $|L|, |L'| \le 4$ (because ss states couple to pp states, which couple to d-orbital and to f-orbital states, and so on), and consider energy gaps between pair states within $2\pi \times 25$ GHz. After diagonalization, the energy map is shown in Fig. 3. In Fig. 3, the red color denotes the population of the state $|70S_{1/2}, m_J = \frac{1}{2}; 70S_{1/2}, m_J = \frac{1}{2}\rangle$ in the diagonalized state; a state denoted by redder color means that if one atom is already in the state $|70S_{1/2}, m_J = \frac{1}{2}\rangle$, it will be easier to populate the state if the other atom is Rydberg pumped via, e.g., the $5P_{3/2}$ intermediate state.

For TSD to hold, we focus on the strong blockade regime where the two-atom Rydberg state shown in Fig. 3 is barely populated. In this case, the *smallest* energy of the diagonalized eigenstate matters, or more accurately, the state with the smallest eigenenergy that can be coupled (marked red). In Fig. 3, we find that, for $\mathcal{L} \in [2.6, 4.6]$ μm, there are mainly three eigenstates, one with a positive energy (labeled state 1), and the other two

TABLE IV. Eigenenergies of the two eigenstates of the dipole-coupled two-atom states that have the largest overlap with the state $|70S_{1/2}, m_J = \frac{1}{2}; 70S_{1/2}, m_J = \frac{1}{2}\rangle$ and that are nearest to zero, labeled state 1 and state 2 in Fig. 3.

	$\mathcal{L}$ (μm)	2.6	3.0	3.6	4.0	4.6
State 1	$V/(2\pi)$ (MHz)	1600	780	340	180	94
State 2	$V/(2\pi)$ (MHz)	−280	−510	−590	−650	−670

with negative energies. For the two that have negative energies, the one we focus on is the state with more overlap with $|ss\rangle \equiv |70S_{1/2}, m_J = \frac{1}{2}; 70S_{1/2}, m_J = \frac{1}{2}\rangle$, whose energy is sometimes lower and sometimes higher than the energy of the other with less population in $|ss\rangle$. The two states we focus on are labeled 1 and 2 in Fig. 3. State 1 has the largest component in $|ss\rangle$: at $\mathcal{L} = \{2.6, 3.0, 3.6, 4.0, 4.6\}$ μm, the amplitude overlap between state 1 and $|ss\rangle$ is $\{0.64, 0.74, 0.84, 0.9, 0.95\}$. For state 2, its overlap with $|ss\rangle$ is $\{0.49, 0.43, 0.32\}$ when $\mathcal{L} = \{2.6, 3.0, 3.6\}$ μm and is negligible when $\mathcal{L}$ is beyond 4.0 μm. The eigenenergies of these two states are listed in Table IV, from which we can see that around $\mathcal{L} = 3.0$ μm the interaction $V = 2\pi \times 510$ can be represented by the eigenenergy of state 2, which is largest for the cases shown in Table IV.

To have $V = 2\pi \times 500$ MHz, the above study shows that placing the two qubits with a distance around $\mathcal{L} = 3.0$ μm seems necessary. With such a distance, the analysis in Ref. [44] shows that the crosstalk error is about 0.5% if the waist ($1/e^2$ intensity radii) of the laser beams is $w = 3.0$ μm. To reduce the crosstalk, it is possible to use super-Gaussian Rydberg beams, as detailed in Ref. [88]. Another possibility is to use higher Rydberg states so that the dipole-dipole interaction can be as large as $V = 2\pi \times 500$ MHz at a larger interatomic distance, and hence the laser-beam crosstalk can be avoided.

If only commonly used Gaussian Rydberg beams are employed for a Rydberg state of principal quantum number around $n = 70$, then smaller values of V can be used for larger interatomic distances so as to avoid crosstalk. For the values $V/(2\pi) \in [50, 400]$ MHz, the fidelity of our gate is shown in Table V, which shows that, with $V = 2\pi \times 100$ MHz, the rotation error is about 1.7×10^{-3} with $T_a = 5$ μK, and the interatomic distance should be around $\mathcal{L} = 4.6$ μm, where crosstalk can be ignored safely ($\Omega'/\Omega \sim e^{-2\mathcal{L}^2/w^2} = 0.009$) if the waists for the lower and upper lasers are both $w = 3.0$ μm. Taking into account the decay error, this means that our gate would have a fidelity of 99.76% with $T_a = 5$ μK at room temperatures.

TABLE V. Rotation errors (scaled up by 10^4; excluding Rydberg-state decay) of the TSD-based CNOT gate by $\Omega_c/2\pi = 3.5$ MHz with different values of V.

$V/(2\pi)$ (MHz)	T (μK)	5	10	15	20	50
50	$10^4 \times \overline{E_{\rm ro}}$	56.5	60.3	64.1	67.8	90.3
100	$10^4 \times \overline{E_{\rm ro}}$	17.0	20.8	24.5	28.3	58.6
200	$10^4 \times \overline{E_{\rm ro}}$	7.09	10.9	14.6	18.4	41.0
300	$10^4 \times \overline{E_{\rm ro}}$	5.25	9.03	12.8	16.6	39.1
400	$10^4 \times \overline{E_{\rm ro}}$	4.61	8.39	12.2	15.9	38.5

APPENDIX C: AMPLITUDE FLUCTUATION OF LASER FIELDS

Our TSD-based CNOT gate requires the Rabi frequencies for the two transitions $|0\rangle \leftrightarrow |r\rangle \leftrightarrow |1\rangle$ to be equal in the target qubit. Here we investigate the impact on the gate fidelity if this condition is not satisfied.

We assume that the Rabi frequency Ω obeys a Gaussian distribution

$$\mathcal{G}(\Omega) = \frac{1}{\sigma\sqrt{2\pi}} e^{-(\Omega-\Omega_k)^2/2\sigma^2} \tag{C1}$$

around the desired value Ω_k, where $k \in \{t1, t2\}$ denotes the two channels $|0\rangle \leftrightarrow |r\rangle$ and $|1\rangle \leftrightarrow |r\rangle$. By using the Gaussian-distributed Rabi frequencies in the target qubit, we can evaluate the averaged fidelity as

$$\overline{E_{\rm ro}} \approx \frac{\sum_{\Omega_{t1}} \sum_{\Omega_{t2}} E_{\rm ro}(\Omega_{t1}, \Omega_{t2}) \mathcal{G}(\Omega_{t1}) \mathcal{G}(\Omega_{t2})}{\sum_{\Omega_{t1}} \sum_{\Omega_{t2}} \mathcal{G}(\Omega_{t1}) \mathcal{G}(\Omega_{t2})}, \tag{C2}$$

where $E_{\rm ro}(\Omega_{t1}, \Omega_{t2})$ is evaluated by using the gate fidelity with Ω_{t1} and Ω_{t2} for the two transitions $|0\rangle \leftrightarrow |r\rangle$ and $|1\rangle \leftrightarrow |r\rangle$. In Eq. (C2), the integration is approximated by the sum over 121 sets of $(\Omega_{t1}, \Omega_{t2})$, each of which applies values $(\Omega - \Omega_k)/\Omega_k \in \{\pm 5, \pm 4, \pm 3, \pm 2, \pm 1, 0\}\sigma$. With $\sigma \in \{0.01, 0.02, 0.03, 0.04, 0.05\}$, the result is shown in Fig. 4. We can see that, with quite a large relative fluctuation in the Gaussian width of 5%, the fidelity is still larger than 99.6%. There is little relation between Doppler dephasing and fluctuation of the Rabi frequency, and we can expect that the gate fidelity can be evaluated by combining Table II and Fig. 4 if the fluctuation of the Rabi frequencies is not quenched.

In Ref. [47], the power fluctuation of the Rydberg lasers was suppressed below 1% for preparing ground-Rydberg entanglement, which means that the Rydberg Rabi frequencies were suppressed to have relative noise below 10%. More than one year later, in Ref. [43], preparation of high-fidelity ground-state entanglement was reported by the same group, which was significant progress. We suppose that the laser noise was even more suppressed in Ref. [43] compared to the earlier experiment in Ref. [47], and thus we consider a relative fluctuation in the Gaussian width of up to 5%.

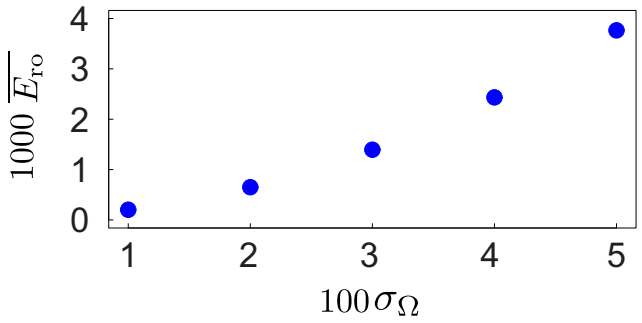

FIG. 4. Fidelity error from the fluctuation in the Rabi frequencies for the two transitions $|0\rangle \leftrightarrow |r\rangle$ and $|1\rangle \leftrightarrow |r\rangle$; the fluctuation obeys a Gaussian distribution of width σ_Ω. The error is 0.003 76 for $\sigma_\Omega = 5\%$.

APPENDIX D: COMPARISON WITH OTHER FAST RYDBERG GATES

It is useful to compare our CNOT gate with other fast entangling methods with Rydberg atoms. The comparisons focus on the physical mechanisms and their application in quantum computing.

A popular method to generate entanglement by Rydberg interactions is to use the EA mechanism [1]. The standard way to use it is a three-pulse sequence for a C_Z gate of the form

$$C_Z = \begin{pmatrix} 1 & 0 & 0 & 0 \\ 0 & -1 & 0 & 0 \\ 0 & 0 & -1 & 0 \\ 0 & 0 & 0 & -1 \end{pmatrix} \tag{D1}$$

in the basis $\{|00\rangle, |01\rangle, |10\rangle, |11\rangle\}$, where the blockade takes effect in the state $|11\rangle$. To use it for quantum computing in the circuit model, the C_Z gate in Eq. (D1) needs single-qubit gates to become a CNOT gate. By this method, an experiment in Ref. [44] realized a CNOT gate of duration more than 100 μs with Rydberg Rabi frequencies $2\pi \times 4.6$ MHz because of the slow single-qubit gates. Physically, this method depends on a missed π phase accumulation in an annihilated Rabi cycle for the input state $|11\rangle$ by the Rydberg blockade.

The other experiment in Ref. [43] used detuned Rabi cycles for entanglement combined with detunings found by optimal control. The method is essentially identical to the interference method proposed in Ref. [81], as can be easily verified by looking at the similar structure of the gate matrix [with the same basis as in Eq. (D1)]

$$C_{\rm phase} = \begin{pmatrix} 1 & 0 & 0 & 0 \\ 0 & e^{i\alpha} & 0 & 0 \\ 0 & 0 & e^{i\alpha} & 0 \\ 0 & 0 & 0 & e^{i\beta} \end{pmatrix} \tag{D2}$$

in Refs. [43,81] (Shi [81] proposed two gates among which the first is quoted here). Compared to the initial interference method, Levine *et al.* [43] used optimal-control-found parameters and phase twist in the Rydberg pumping within the blockade regime so as to realize $2\alpha - \beta = \pi$ (and thus the gate in Ref. [43] can be called a C_Z-like gate). Because of the detuned Rabi cycles used, there is no way to realize a gate with $\{\alpha, \beta\}/\pi = \{N_1, N_2\}$, where N_j is an integer with $j = 1, 2$. To use it in quantum computing, several single-qubit gates must be used to transform the gate in Ref. [43] to the CNOT gate, so their final CNOT gate duration was more than 4 μs with Rydberg Rabi frequencies $2\pi \times 3.5$ MHz. Without using the detuned Rabi cycles, the method in Ref. [43] cannot work. The physical mechanism of Ref. [43] is that dynamical phases in detuned Rabi cycles are accumulated.

In order to compare with the gates in Eqs. (D1) and (D2) that have a diagonal form, the TSD-based CNOT gate in the basis $\{|00\rangle, |01\rangle, |10\rangle, |11\rangle\}$ can be rewritten as

$$C_{\rm TSD} = \begin{pmatrix} 1 & 0 & 0 & 0 \\ 0 & 1 & 0 & 0 \\ 0 & 0 & -1 & 0 \\ 0 & 0 & 0 & 1 \end{pmatrix} \tag{D3}$$

with the basis $\{|0\bar{0}\rangle, |0\bar{1}\rangle, |1\bar{0}\rangle, |1\bar{1}\rangle\}$, where $|\bar{1}(\bar{0})\rangle = (|0\rangle \pm |1\rangle)/\sqrt{2}$. The CNOT gate duration would be less than 0.4 μs with Rydberg Rabi frequencies less than or equal to $2\pi \times 3.5$ MHz by the TSD method. The blockade interaction is in $|1\bar{1}\rangle$ and the pumping of the target qubit induces a transition from $|1\bar{1}\rangle$ to $|\mathscr{S}_+\rangle \equiv (\Omega_c|r\bar{1}\rangle + \sqrt{2}\Omega_t|1r\rangle)/\overline{\Omega}$ with a Rabi frequency $\overline{\Omega} = \sqrt{\Omega_c^2 + 2\Omega_t^2}$ while further excitation to $|rr\rangle$ is blocked. Each of the two pulses in the TSD-based CNOT sequence induces a complete 2π rotation $|1\bar{1}\rangle \to -i|\mathscr{S}_+\rangle \to -|1\bar{1}\rangle$ that leads to a π phase change to $|1\bar{1}\rangle$. The change of the sign of Ω_t between the two pulses does not change this picture, and thus a total phase 2π is accumulated in $|1\bar{1}\rangle$. Since $e^{2i\pi} = 1$, $|1\bar{1}\rangle$ acquires no phase term in practice. On the other hand, the input state $|1\bar{0}\rangle$ only experiences two π pulses (i.e., a 2π pulse) in the control qubit that results in a π phase change to it. The pumping of the target qubit experiences spin echo for the input state $|0\bar{1}\rangle$; thus, no phase appears for it. So, the physical mechanism of the gate in Eq. (D3) is fundamentally different from those in Eqs. (D1) and (D2); in fact, the drastically different forms of the three gate maps reveal this. To conclude, Eq. (D1) relies on a missed π phase change in an annihilated Rabi cycle, Eq. (D2) relies on three phase changes in three detuned Rabi cycles, and Eq. (D3) relies on a π phase change in a resonant Rabi cycle. For quantum computing, the gate in Eq. (D3) is exactly a CNOT gate in the basis $\{|00\rangle, |01\rangle, |10\rangle, |11\rangle\}$, and thus is more useful compared to Eqs. (D1) and (D2).

Because a phase twist is used in realizing both Eqs. (D2) and (D3), we may guess that they are similar. But the following facts show their distinct physics: (i) detuned

Rydberg pumping is used in Eq. (D2), but resonant Rydberg pumping is used in Eq. (D3); (ii) three input states acquire phase terms in Eq. (D2), but only one input state acquires a phase term in Eq. (D3); (iii) the population in the Rydberg state can reach 1 for the fourth input state $|1\bar{1}\rangle$ in Eq. (D3), while there is no way to realize such an effect in Eq. (D2). This last effect basically means that the mechanism for realizing Eq. (D3) can be used to realize a high-fidelity multiqubit gate: we can use TSD to excite the input state $|1\bar{1}\rangle$ to $|\mathscr{S}_+\rangle$ that can block the Rydberg pumping in a nearby atom (of course, care must be taken for the design of such a gate). Note that the three-qubit gate in Ref. [43] requires exciting the two edge atoms to block the Rydberg pumping in the middle atom that results in error due to the residual blockade between the two edge atoms. For the method in Eq. (D2), detuned Rabi cycles are used and they cannot excite *one* Rydberg excitation in the blocked excitation [for the input state $|11\rangle$ in Eq. (D2)], and thus it is not possible to extend the method in Eq. (D2) to a high-fidelity multiqubit gate. This means that the underlying physics in Eq. (D3) is different from that of Eq. (D2).

Note that the basis transform used to write the TSD-based CNOT gate matrix in Eq. (D2) is used only for clarifying the physics, but not for practical use since in a large-scale quantum computer the way to encode quantum information is based on a commonly used qubit basis in all registers (otherwise, the information loading and retrieving faces trouble). For example, to initialize the atomic arrays, the quantization axis is fixed by applying, e.g., an external magnetic field, and the qubit states $|0\rangle$ and $|1\rangle$ are chosen from two hyperfine levels with different energies. So, the states $|\bar{1}(\bar{0})\rangle = (|0\rangle \pm |1\rangle)/\sqrt{2}$ are no longer eigenstates because of the applied external fields, and new state detection schemes need to be designed. In a large-scale quantum computer, to play the role of control or target is not fixed for any qubit: a computational task is divided into a series of unitary operations, and the same qubit sometimes serves as a control and sometimes a target in the different unitary operations. This means that if one uses a hybrid coding with $|0(1)\rangle$ for the control and $|\bar{1}(\bar{0})\rangle$ for the target, an exceedingly large amount of transforming operations between $|0(1)\rangle$ and $|\bar{1}(\bar{0})\rangle$ should be used in the quantum circuit. So, it is impractical to use $|0(1)\rangle$ for information coding in the control, and to use $|\bar{1}(\bar{0})\rangle$ for information coding in the target; for a proof-of-principle study either in theory or in experiment, it may be of interest, but not for a realistic large-scale quantum computer.

APPENDIX E: ac STARK SHIFTS

There is a detailed study about the ac Stark shifts in a two-photon Rydberg excitation in Ref. [41]. Appendix B of Ref. [41] presents a detailed calculation of the ac Stark shifts accounting for the hyperfine splitting of the intermediate state, where one can find that compensation of the ac Stark shifts is feasible. Below, we ignore the hyperfine splitting of the intermediate state to give a brief introduction. More details can be found in Ref. [41].

Here, we choose the qubit states $|1\rangle = |6S_{1/2}, F = 3, m_F = 3\rangle$ and $|0\rangle = |6S_{1/2}, F = 4, m_F = 4\rangle$ of cesium. The state $|1\rangle$ is driven to $|p\rangle$ (in the $7P_{1/2}$ manifold) with laser fields that are left-hand circularly polarized (note that this is a little different from Ref. [41]), which is further excited to $|r\rangle = |82S_{1/2}, m_J, m_I\rangle$. The Hamiltonian for a two-photon Rydberg excitation is (in this section we explicitly put $\hbar$ in Hamiltonians)

$$\hat{H}_{2\text{-pho};0} = \hbar[\Omega_1|p\rangle\langle 1|/2 + \Omega_2|r\rangle\langle p|/2 + \text{H.c.}] + \hbar\Delta|p\rangle\langle p|, \tag{E1}$$

where Δ is defined as the frequency of the laser field deducted by the frequency of the atomic transition. Note that we have not included the nonresonant shift in the equation above. When Δ is very large compared to the decay rate of $|p\rangle$, the intermediate state can be adiabatically eliminated, leading to

$$\hat{H}_{2\text{-pho}} = \hbar\{[\Omega_{\text{eff}}|r\rangle\langle 1|/2 + \text{H.c.}] + \Delta_r|r\rangle\langle r| + \Delta_{q1}|1\rangle\langle 1|\}, \tag{E2}$$

where $\Omega_{\text{eff}} = \Omega_1\Omega_2/(2\Delta)$, and according to Ref. [41] the effective detuning at the level $|r\rangle$ is

$$\Delta_r(\omega_1, \omega_2, \Delta, \mathcal{E}_1, \mathcal{E}_2) = \frac{\Omega_2^2}{4\Delta} - \frac{e^2}{4m_e\hbar}\left(\frac{\mathcal{E}_1^2}{\omega_1^2} + \frac{\mathcal{E}_2^2}{\omega_2^2}\right), \tag{E3}$$

where e is the elementary charge, m_e is the mass of the electron, and ω_j and $\mathcal{E}_j$ are the frequency and electric field amplitude of the laser field, where $j = 1$ and 2 for the lower and upper transitions, respectively. Similarly, for the ground state, the effective detuning is

$$\Delta_{q1}(\omega_1, \omega_2, \Delta, \mathcal{E}_1, \mathcal{E}_2) = \frac{\Omega_1^2}{4\Delta} - \frac{1}{4\hbar}(\alpha_1\mathcal{E}_1^2 + \alpha_2\mathcal{E}_2^2), \tag{E4}$$

where α_1 and α_2 are the nonresonant polarizabilities from the lower and upper fields that can be calculated via the sum over transitions to other states except the intermediate state $|p\rangle$. Meanwhile, there is a shift on the ground state $|0\rangle$,

$$\Delta_{q0}(\omega_1, \omega_2, \Delta, \mathcal{E}_1, \mathcal{E}_2) = \frac{\mathscr{C}^2\Omega_1^2}{4(\Delta + \omega_q)} - \frac{1}{4\hbar}(\alpha_1\mathcal{E}_1^2 + \alpha_2\mathcal{E}_2^2), \tag{E5}$$

where ω_q is the frequency separation between $|0\rangle$ and $|1\rangle$, and $\mathscr{C}$ is a factor determined by the selection

rules. Because $\alpha_2/\alpha_1 = -16.3$ and α_1 is negative, the off-resonant shift will be negative, and thus it is necessary for the resonant shift to be positive. So, both Δ in Eq. (E4) and $\Delta + \omega_q$ in Eq. (E5) will be positive, which further means that $\mathscr{C}^2$ will be larger than 1.

For the case when Δ is much larger than the hyperfine splitting of the intermediate $7P_{1/2}$ state, we ignore its hyperfine splitting and then it can be written as $|7P_{1/2}, m_J, m_I\rangle$. When right-hand polarized fields are used for coupling qubit states and the $7P_{1/2}$ states, the square of the ratio of the coupling between $|0\rangle$ and $|p\rangle$ and that between $|1\rangle$ and $|p\rangle$ is

$$\mathscr{C}^2 = \frac{\sum_{m_J,m_I}(\sum_{m_e} C^{1/2,1,1/2}_{m_J,1,m_e} C^{1/2,7/2,4}_{m_e,m_I,0})^2}{\sum_{m_J,m_I}(\sum_{m_e} C^{1/2,1,1/2}_{m_J,1,m_e} C^{1/2,7/2,3}_{m_e,m_I,0})^2}, \tag{E6}$$

which is 8. To shift $\Delta_r(\omega_1, \omega_2, \Delta, \mathcal{E}_1, \mathcal{E}_2)$ to zero, one can simply adjust the frequency of the laser fields for addressing the upper transition. To compensate the Stark shifts at $|0\rangle$ and $|1\rangle$, Eqs. (E4) and (E5) indicate that $\mathscr{C}^2 = 1 + \omega_q/\Delta$, meaning that we choose $\Delta = \omega_q/(\mathscr{C}^2 - 1) \approx 2\pi \times 1.3$ GHz (for rubidium, it would be $2\pi \times 0.97$ GHz), which is near to the values used in experiments [39,41]. With $\Delta = \omega_q/(\mathscr{C}^2 - 1)$ satisfied, an appropriate set of $(\Delta, \mathcal{E}_1, \mathcal{E}_2)$ satisfying Eq. (E4) would satisfy Eq. (E5), too. With the given data for the radial coupling between ground and $|p\rangle$ states and the values of $\alpha_{1,2}$ (see p. 6 of Ref. [41]), Eq. (E4) reduces to $\overline{\Delta}[16.3(\mathcal{E}_2/\mathcal{E}_1)^2 - 1] = 2.98$, where $\overline{\Delta} = \Delta \times 10^{-9}$ s, which can be used to set up the ratio $|\mathcal{E}_2/\mathcal{E}_1|$.

We have shown the method to compensate the Stark shifts if pumping applies only to the transition $|1\rangle \leftrightarrow |r\rangle$. For the target qubit, there will be another transition required, $|0\rangle \leftrightarrow |r\rangle$. Then, four fields lead to Stark shifts in the two qubit states (two equations), and there is a condition that the Rabi frequencies for $|0(1)\rangle \leftrightarrow |r\rangle$ must be equal (a third equation). Moreover, there will be two detunings at the intermediate states for these two transitions. Altogether there are three equations for six variables and hence the problem is solvable. The Stark shift at $|r\rangle$ can be compensated by adjusting the central frequencies of the laser fields. So, Eq. (A3), or Eq. (3), can be realized.

For one-photon excitation of p-orbital Rydberg states, the off-resonant ac Stark shift on $|0\rangle$ or $|1\rangle$ from the resonant field is positive, but one can use another field of larger wavelength to induce a negative shift. Then, a similar set of equations to Eqs. (E4) and (E5) can be established to compensate the Stark shifts. For the shift on the Rydberg state, one can shift the wavelength of the laser field to recover the resonance condition for $|r\rangle$.

APPENDIX F: CNOT GATE IN OTHER SYSTEMS

It is useful to compare the speed of the CNOT gate in different physical systems by using the ratio $\Xi = T_{\rm coh}/T_g$, where $T_{\rm coh}$ is the coherence time (pure spin dephasing T_2 or the inhomogeneously broadened T_2^*), and T_g is the duration of the CNOT gate. First, for neutral atom qubit systems, in Ref. [78] a coherence time of 7 s has been measured (see the left column of p. 2 of Ref. [78]) in a large neutral atom array. Wang *et al.* [78] realized such a coherence time so as to have high fidelity in the single-qubit gates that had gate durations 80 μs; in principle, much longer coherence times can be achieved. To have a conserved estimation, we assume that a coherence time of 7 s for neutral atoms. With the protocol in this manuscript, the CNOT gate duration would be about 0.3 μs with Rydberg Rabi frequencies like those realized in Refs. [43,44]. Then, the figure of merit would be $\Xi = 2.3 \times 10^7$.

Second, for trapped ions, several most advanced results can be inferred from the literature. However, one should bare in mind that some fast entangling gates are not CNOT gates. Any two-qubit entangling gate can be repeated several times to form a CNOT gate when assisted by single-qubit gates, as demonstrated in Ref. [57], but the CNOT gate is the gate directly helpful to quantum computation in the circuit model [56–60]. So, we focus on data for trapped ions with CNOT gates demonstrated. (i) In Ref. [63], Bell states of trapped ions were created with gate times of 27.4 μs. The coherence times were not mentioned in Ref. [63]. However, near the end of Ref. [63] it stated coherence times of 60 s, indicating that the coherence times of their qubits were around 60 s. So the figure of merit would be 60 s/(27.4 μs), which is about $\Xi = 2.2 \times 10^6$. (ii) In Ref. [64], Bell states of trapped ions were prepared with pulses of durations from 50 μs to 100 μs; very short gate times of about 3.8 μs were also given. In the supplemental material of Ref. [64], it showed that the coherence time was about 6 s. So the figure of merit was 6 s/(3.8 μs), which is about $\Xi = 1.6 \times 10^6$. (iii) In Ref. [65], Bell states of trapped ions were prepared with pulses of duration about 30 μs (Fig. 6 of Ref. [65] showed gates with durations even longer), and the coherence time was about 1.5 s. So the figure of merit would be 1.5 s/(30 μs), which is about $\Xi = 5 \times 10^4$.

Third, for superconducting qubits, very fast CNOT gates were reported in Ref. [70]. The energy relaxation time T_1 is usually shorter than the phase coherence time T_2^* in superconducting circuits. In Ref. [70] the measured value of T_1 was 20–40 μs and values up to 57 μs were recorded. The supplementary information of Ref. [70] showed that the C_Z-gate durations can be as short as 38 ns, and the single-qubit gate times can be as small as 10 ns. So the duration of a CNOT gate can be $T_g = 58$ ns, leading to the figure of merit $\Xi = 10^3$. Suppose that the fast gate in Ref. [70] was realized in the superconducting system with a longer coherence time $T_1 = 70$ μs [89]; then the figure of merit $\Xi = 1.2 \times 10^3$ is still much smaller than those in neutral atoms.

Concerning the ratio between the coherence time and the CNOT gate duration, the above comparison shows that TSD

makes neutral atoms advantageous compared to trapped ions and superconducting systems.

[1] D. Jaksch, J. I. Cirac, P. Zoller, S. L. Rolston, R. Côté, and M. D. Lukin, Fast Quantum Gates for Neutral Atoms, Phys. Rev. Lett. **85**, 2208 (2000).

[2] M. D. Lukin, M. Fleischhauer, R. Cote, L. M. Duan, D. Jaksch, J. I. Cirac, and P. Zoller, Dipole Blockade and Quantum Information Processing in Mesoscopic Atomic Ensembles, Phys. Rev. Lett. **87**, 037901 (2001).

[3] M. Saffman, T. G. Walker, and K. Mølmer, Quantum information with Rydberg atoms, Rev. Mod. Phys. **82**, 2313 (2010).

[4] M. Saffman, Quantum computing with atomic qubits and Rydberg interactions: Progress and challenges, J. Phys. B **49**, 202001 (2016).

[5] D. S. Weiss and M. Saffman, Quantum computing with neutral atoms, Phys. Today **70**, No. 7, 44 (2017).

[6] O. Firstenberg, C. S. Adams, and S. Hofferberth, Nonlinear quantum optics mediated by Rydberg interactions, J. Phys. B **49**, 152003 (2016).

[7] C. S. Adams, J. D. Pritchard, and J. P. Shaffer, Rydberg atom quantum technologies, J. Phys. B **53**, 012002 (2020).

[8] A. Browaeys and T. Lahaye, Many-body physics with individually controlled Rydberg atoms, Nat. Phys. **16**, 132 (2020).

[9] J. H. Gurian, P. Cheinet, P. Huillery, A. Fioretti, J. Zhao, P. L. Gould, D. Comparat, and P. Pillet, Observation of a Resonant Four-Body Interaction in Cold Cesium Rydberg Atoms, Phys. Rev. Lett. **108**, 023005 (2012).

[10] D. B. Tretyakov, I. I. Beterov, E. A. Yakshina, V. M. Entin, I. I. Ryabtsev, P. Cheinet, and P. Pillet, Observation of the Borromean Three-Body Förster Resonances for Three Interacting Rb Rydberg Atoms, Phys. Rev. Lett. **119**, 173402 (2017).

[11] S. De Léséleuc, V. Lienhard, P. Scholl, D. Barredo, S. Weber, N. Lang, H. P. Büchler, T. Lahaye, and A. Browaeys, Observation of a symmetry-protected topological phase of interacting bosons with Rydberg atoms, Science **365**, 775 (2019).

[12] P. Schauß, J. Zeiher, T. Fukuhara, S. Hild, M. Cheneau, T. Macrì, T. Pohl, I. Bloch, and C. Gross, Crystallization in Ising quantum magnets, Science **347**, 1455 (2015).

[13] H. Labuhn, D. Barredo, S. Ravets, S. de Léséleuc, T. Macrì, T. Lahaye, and A. Browaeys, A highly-tunable quantum simulator of spin systems using two-dimensional arrays of single Rydberg atoms, Nature **534**, 667 (2016).

[14] J. Zeiher, R. V. Bijnen, P. Schauß, S. Hild, J.-Y. Choi, T. Pohl, I. Bloch, and C. Gross, Many-body interferometry of a Rydberg-dressed spin lattice, Nat. Phys. **12**, 1095 (2016).

[15] J. Zeiher, J.-Y. Choi, A. Rubio-Abadal, T. Pohl, R. van Bijnen, I. Bloch, and C. Gross, Coherent Many-Body Spin Dynamics in a Long-Range Interacting Ising Chain, Phys. Rev. X **7**, 041063 (2017).

[16] H. Bernien, S. Schwartz, A. Keesling, H. Levine, A. Omran, H. Pichler, S. Choi, A. S. Zibrov, M. Endres, M. Greiner, V. Vuletic, and M. D. Lukin, Probing many-body dynamics on a 51-atom quantum simulator, Nature **551**, 579 (2017).

[17] S. de Léséleuc, S. Weber, V. Lienhard, D. Barredo, H. P. Büchler, T. Lahaye, and A. Browaeys, Accurate Mapping of Multilevel Rydberg Atoms on Interacting Spin-1/2 Particles for the Quantum Simulation of Ising Models, Phys. Rev. Lett. **120**, 113602 (2018).

[18] E. Guardado-Sanchez, P. T. Brown, D. Mitra, T. Devakul, D. A. Huse, P. Schauß, and W. S. Bakr, Probing the Quench Dynamics of Antiferromagnetic Correlations in a 2D Quantum Ising Spin System, Phys. Rev. X **8**, 021069 (2018).

[19] H. Kim, Y.-J. Park, K. Kim, H. S. Sim, and J. Ahn, Detailed Balance of Thermalization Dynamics in Rydberg Atom Quantum Simulators, Phys. Rev. Lett. **120**, 180502 (2018).

[20] A. Keesling, A. Omran, H. Levine, H. Bernien, H. Pichler, S. Choi, R. Samajdar, S. Schwartz, P. Silvi, S. Sachdev, P. Zoller, M. Endres, M. Greiner, V. Vuletić, and M. D. Lukin, Quantum Kibble–Zurek mechanism and critical dynamics on a programmable Rydberg simulator, Nature **568**, 207 (2019).

[21] D.-S. Ding, H. Busche, B.-S. Shi, G.-C. Guo, and C. S. Adams, Phase Diagram and Self-Organizing Dynamics in a Thermal Ensemble of Strongly Interacting Rydberg Atoms, Phys. Rev. X **10**, 21023 (2020).

[22] V. Borish, O. Marković, J. A. Hines, S. V. Rajagopal, and M. Schleier-Smith, Transverse-Field Ising Dynamics in a Rydberg-Dressed Atomic Gas, Phys. Rev. Lett. **124**, 063601 (2020).

[23] Y. O. Dudin and A. Kuzmich, Strongly interacting Rydberg excitations of a cold atomic gas, Science **336**, 887 (2012).

[24] T. Peyronel, O. Firstenberg, Q.-Y. Liang, S. Hofferberth, A. V. Gorshkov, T. Pohl, M. D. Lukin, and V. Vuletić, Quantum nonlinear optics with single photons enabled by strongly interacting atoms, Nature **488**, 57 (2012).

[25] O. Firstenberg, T. Peyronel, Q.-Y. Liang, A. V. Gorshkov, M. D. Lukin, and V. Vuletić, Attractive photons in a quantum nonlinear medium, Nature **488**, 57 (2013).

[26] L. Li, Y. O. Dudin, and A. Kuzmich, Entanglement between light and an optical atomic excitation, Nature **498**, 466 (2013).

[27] H. Gorniaczyk, C. Tresp, J. Schmidt, H. Fedder, and S. Hofferberth, Single-Photon Transistor Mediated by Interstate Rydberg Interactions, Phys. Rev. Lett. **113**, 053601 (2014).

[28] S. Baur, D. Tiarks, G. Rempe, and S. Dürr, Single-Photon Switch Based on Rydberg Blockade, Phys. Rev. Lett. **112**, 073901 (2014).

[29] D. Tiarks, S. Baur, K. Schneider, S. Dürr, and G. Rempe, Single-Photon Transistor Using a Förster Resonance, Phys. Rev. Lett. **113**, 053602 (2014).

[30] J. Li, M.-T. Zhou, B. Jing, X.-J. Wang, S.-J. Yang, X. Jiang, K. Mølmer, X.-H. Bao, and J.-W. Pan, Hong-Ou-Mandel Interference between Two Deterministic Collective Excitations in an Atomic Ensemble, Phys. Rev. Lett. **117**, 180501 (2016).

[31] H. Busche, P. Huillery, S. W. Ball, T. Ilieva, M. P. A. Jones, and C. S. Adams, Contactless nonlinear optics mediated by long-range Rydberg interactions, Nat. Phys. **13**, 655 (2017).

[32] F. Ripka and T. Pfau, A room-temperature single-photon source based on strongly interacting Rydberg atoms, Science **449**, 446 (2018).

[33] Q.-Y. Liang, A. V. Venkatramani, S. H. Cantu, T. L. Nicholson, M. J. Gullans, A. V. Gorshkov, J. D. Thompson, C. Chin, M. D. Lukin, and V. Vuleti, Observation of three-photon bound states in a quantum nonlinear medium, Science **786**, 783 (2018).

[34] J. Li, M.-T. Zhou, C.-W. Yang, P.-F. Sun, J.-L. Liu, X.-H. Bao, and J.-W. Pan, Semi-Deterministic Entanglement between a Single Photon and an Atomic Ensemble, Phys. Rev. Lett. **123**, 140504 (2019).

[35] J. D. Thompson, T. L. Nicholson, Q.-Y. Liang, S. H. Cantu, A. V. Venkatramani, S. Choi, I. A. Fedorov, D. Viscor, T. Pohl, M. D. Lukin, and V. Vuletić, Symmetry-protected collisions between strongly interacting photons, Nature **542**, 206 (2017).

[36] M. Ebert, M. Kwon, T. G. Walker, and M. Saffman, Coherence and Rydberg Blockade of Atomic Ensemble Qubits, Phys. Rev. Lett. **115**, 093601 (2015).

[37] A. Omran, H. Levine, A. Keesling, G. Semeghini, T. T. Wang, S. Ebadi, H. Bernien, A. S. Zibrov, H. Pichler, S. Choi, J. Cui, M. Rossignolo, P. Rembold, S. Montangero, T. Calarco, M. Endres, M. Greiner, V. Vuletić, and M. D. Lukin, Generation and manipulation of Schrödinger cat states in Rydberg atom arrays, Science **365**, 570 (2019).

[38] T. Wilk, A. Gaëtan, C. Evellin, J. Wolters, Y. Miroshnychenko, P. Grangier, and A. Browaeys, Entanglement of Two Individual Neutral Atoms Using Rydberg Blockade, Phys. Rev. Lett. **104**, 010502 (2010).

[39] L. Isenhower, E. Urban, X. L. Zhang, A. T. Gill, T. Henage, T. A. Johnson, T. G. Walker, and M. Saffman, Demonstration of a Neutral Atom Controlled-NOT Quantum Gate, Phys. Rev. Lett. **104**, 010503 (2010).

[40] X. L. Zhang, L. Isenhower, A. T. Gill, T. G. Walker, and M. Saffman, Deterministic entanglement of two neutral atoms via Rydberg blockade, Phys. Rev. A **82**, 030306(R) (2010).

[41] K. M. Maller, M. T. Lichtman, T. Xia, Y. Sun, M. J. Piotrowicz, A. W. Carr, L. Isenhower, and M. Saffman, Rydberg-blockade controlled-not gate and entanglement in a two-dimensional array of neutral-atom qubits, Phys. Rev. A **92**, 022336 (2015).

[42] Y. Zeng, P. Xu, X. He, Y. Liu, M. Liu, J. Wang, D. J. Papoular, G. V. Shlyapnikov, and M. Zhan, Entangling Two Individual Atoms of Different Isotopes via Rydberg Blockade, Phys. Rev. Lett. **119**, 160502 (2017).

[43] H. Levine, A. Keesling, G. Semeghini, A. Omran, T. T. Wang, S. Ebadi, H. Bernien, M. Greiner, V. Vuletić, H. Pichler, and M. D. Lukin, Parallel Implementation of High-Fidelity Multi-Qubit Gates with Neutral Atoms, Phys. Rev. Lett. **123**, 170503 (2019).

[44] T. M. Graham, M. Kwon, B. Grinkemeyer, Z. Marra, X. Jiang, M. T. Lichtman, Y. Sun, M. Ebert, and M. Saffman, Rydberg Mediated Entanglement in a Two-Dimensional Neutral Atom Qubit Array, Phys. Rev. Lett. **123**, 230501 (2019).

[45] I. S. Madjarov, J. P. Covey, A. L. Shaw, J. Choi, A. Kale, A. Cooper, H. Pichler, V. Schkolnik, J. R. Williams, and M. Endres, High-fidelity entanglement and detection of alkaline-earth Rydberg atoms, Nat. Phys. **16**, 857 (2020).

[46] Y.-Y. Jau, A. M. Hankin, T. Keating, I. H. Deutsch, and G. W. Biedermann, Entangling atomic spins with a Rydberg-dressed spin-flip blockade, Nat. Phys. **12**, 71 (2016).

[47] H. Levine, A. Keesling, A. Omran, H. Bernien, S. Schwartz, A. S. Zibrov, M. Endres, M. Greiner, V. Vuletić, and M. D. Lukin, High-Fidelity Control and Entanglement of Rydberg Atom Qubits, Phys. Rev. Lett. **121**, 123603 (2018).

[48] C. J. Picken, R. Legaie, K. McDonnell, and J. D. Pritchard, Entanglement of neutral-atom qubits with long ground-Rydberg coherence times, Quantum Sci. Technol. **4**, 015011 (2019).

[49] D. Tiarks, S. Schmidt-Eberle, T. Stolz, G. Rempe, and S. Dürr, A photon–photon quantum gate based on Rydberg interactions, Nat. Phys. **15**, 124 (2019).

[50] H. Jo, Y. Song, M. Kim, and J. Ahn, Rydberg Atom Entanglements in the Weak Coupling Regime, Phys. Rev. Lett. **124**, 33603 (2020).

[51] C. Ates, T. Pohl, T. Pattard, and J. M. Rost, Antiblockade in Rydberg Excitation of an Ultracold Lattice Gas, Phys. Rev. Lett. **98**, 023002 (2007).

[52] T. Amthor, C. Giese, C. S. Hofmann, and M. Weidemüller, Evidence of Antiblockade in an Ultracold Rydberg Gas, Phys. Rev. Lett. **104**, 013001 (2010).

[53] M. A. Nielsen and I. L. Chuang, *Quantum Computation and Quantum Information* (Cambridge University Press, Cambridge, 2000).

[54] C. P. Williams, in *Explorations in Quantum Computing*, edited by D. Gries and F. B. Schneider, Texts in Computer Science (Springer-Verlag, London, 2011), 2nd ed.

[55] T. D. Ladd, F. Jelezko, R. Laflamme, Y. Nakamura, C. Monroe, and J. L. O'Brien, Quantum computers, Nature **464**, 45 (2010).

[56] P. W. Shor, Polynomial-time algorithms for prime factorization and discrete logarithms on a quantum computer, SIAM J. Comput. **26**, 1484 (1997).

[57] M. J. Bremner, C. M. Dawson, J. L. Dodd, A. Gilchrist, A. W. Harrow, D. Mortimer, M. A. Nielsen, and T. J. Osborne, Practical Scheme for Quantum Computation with Any Two-Qubit Entangling Gate, Phys. Rev. Lett. **89**, 247902 (2002).

[58] V. V. Shende, I. L. Markov, and S. S. Bullock, Minimal universal two-qubit controlled-NOT-based circuits, Phys. Rev. A **69**, 062321 (2004).

[59] A. Peruzzo, J. McClean, P. Shadbolt, M. H. Yung, X. Q. Zhou, P. J. Love, A. Aspuru-Guzik, and J. L. O'Brien, A variational eigenvalue solver on a photonic quantum processor, Nat. Commun. **5**, 4213 (2014).

[60] S. Debnath, N. M. Linke, C. Figgatt, K. A. Landsman, K. Wright, and C. Monroe, Demonstration of a small programmable quantum computer with atomic qubits, Nature **536**, 63 (2016).

[61] J. I. Cirac and P. Zoller, Quantum Computations with Cold Trapped Ions, Phys. Rev. Lett. **74**, 4091 (1995).

[62] A. Sørensen and K. Mølmer, Quantum Computation with Ions in Thermal Motion, Phys. Rev. Lett. **82**, 1971 (1999).

[63] C. J. Ballance, V. M. Schafer, J. P. Home, D. J. Szwer, S. C. Webster, D. T. C. Allcock, N. M. Linke, T. P. Harty, D. P. L. A. Craik, D. N. Stacey, A. M. Steane, and D. M. Lucas, Hybrid quantum logic and a test of Bell's inequality using two different atomic species, Nature **528**, 384 (2015).

[64] C. J. Ballance, T. P. Harty, N. M. Linke, M. A. Sepiol, and D. M. Lucas, High-Fidelity Quantum Logic Gates Using Trapped-Ion Hyperfine Qubits, Phys. Rev. Lett. **117**, 060504 (2016).

[65] J. P. Gaebler, T. R. Tan, Y. Lin, Y. Wan, R. Bowler, A. C. Keith, S. Glancy, K. Coakley, E. Knill, D. Leibfried, and D. J. Wineland, High-Fidelity Universal Gate Set for Be^+ Ion Qubits, Phys. Rev. Lett. **117**, 060505 (2016).

[66] V. M. Schäfer, C. J. Ballance, K. Thirumalai, L. J. Stephenson, T. G. Ballance, A. M. Steane, and D. M. Lucas, Fast quantum logic gates with trapped-ion qubits, Nature **555**, 75 (2018).

[67] C. Zhang, F. Pokorny, W. Li, G. Higgins, A. Pöschl, I. Lesanovsky, and M. Hennrich, Submicrosecond entangling gate between trapped ions via Rydberg interaction, Nature **580**, 345 (2020).

[68] J. Q. You and F. Nori, Superconducting circuits and quantum information, Phys. Today **58**, No. 11, 42 (2005).

[69] M. H. Devoret and R. J. Schoelkopf, Superconducting circuits for quantum information: An outlook, Science **339**, 1169 (2013).

[70] R. Barends *et al.*, Superconducting quantum circuits at the surface code threshold for fault tolerance, Nature **508**, 500 (2014).

[71] T. G. Walker and M. Saffman, Consequences of Zeeman degeneracy for the van der Waals blockade between Rydberg atoms, Phys. Rev. A **77**, 032723 (2008).

[72] M. Saffman and T. G. Walker, Analysis of a quantum logic device based on dipole-dipole interactions of optically trapped Rydberg atoms, Phys. Rev. A **72**, 022347 (2005).

[73] X.-F. Shi, Accurate Quantum Logic Gates by Spin Echo in Rydberg Atoms, Phys. Rev. Appl. **10**, 034006 (2018).

[74] X.-F. Shi, Single-site Rydberg addressing in 3D atomic arrays for quantum computing with neutral atoms, J. Phys. B **53**, 054002 (2020).

[75] X.-F. Shi, Deutsch, Toffoli, and CNOT Gates via Rydberg Blockade of Neutral Atoms, Phys. Rev. Appl. **9**, 051001 (2018).

[76] M. Müller, I. Lesanovsky, H. Weimer, H. P. Büchler, and P. Zoller, Mesoscopic Rydberg Gate Based on Electromagnetically Induced Transparency, Phys. Rev. Lett. **102**, 170502 (2009).

[77] T. Xia, M. Lichtman, K. Maller, A. W. Carr, M. J. Piotrowicz, L. Isenhower, and M. Saffman, Randomized Benchmarking of Single-Qubit Gates in a 2D Array of Neutral-Atom Qubits, Phys. Rev. Lett. **114**, 100503 (2015).

[78] Y. Wang, A. Kumar, T.-Y. Wu, and D. S. Weiss, Single-qubit gates based on targeted phase shifts in a 3D neutral atom array, Science **352**, 1562 (2016).

[79] D. D. Yavuz, P. B. Kulatunga, E. Urban, T. A. Johnson, N. Proite, T. Henage, T. G. Walker, and M. Saffman, Fast Ground State Manipulation of Neutral Atoms in Microscopic Optical Traps, Phys. Rev. Lett. **96**, 063001 (2006).

[80] M. P. A. Jones, J. Beugnon, A. Gaëtan, J. Zhang, G. Messin, A. Browaeys, and P. Grangier, Fast quantum state control of a single trapped neutral atom, Phys. Rev. A **75**, 040301(R) (2007).

[81] X.-F. Shi, Fast, Accurate, and Realizable Two-Qubit Entangling Gates by Quantum Interference in Detuned Rabi Cycles of Rydberg Atoms, Phys. Rev. Appl. **11**, 044035 (2019).

[82] I. I. Beterov, I. I. Ryabtsev, D. B. Tretyakov, and V. M. Entin, Quasiclassical calculations of blackbody-radiation-induced depopulation rates and effective lifetimes of Rydberg nS, nP, and nD alkali-metal atoms with $n \leq 80$, Phys. Rev. A **79**, 052504 (2009).

[83] X.-F. Shi, Suppressing Motional Dephasing of Ground-Rydberg Transition for High-Fidelity Quantum Control with Neutral Atoms, Phys. Rev. Appl. **13**, 024008 (2020).

[84] X. L. Zhang, A. T. Gill, L. Isenhower, T. G. Walker, and M. Saffman, Fidelity of a Rydberg-blockade quantum gate from simulated quantum process tomography, Phys. Rev. A **85**, 042310 (2012).

[85] M. Saffman, I. I. Beterov, A. Dalal, E. J. Paez, and B. C. Sanders, Symmetric Rydberg controlled-Z gates with adiabatic pulses control target, Phys. Rev. A **101**, 62309 (2020).

[86] L. H. Pedersen, N. M. Møller, and K. Mølmer, Fidelity of quantum operations, Phys. Lett. A **367**, 47 (2007).

[87] N. Šibalić, J. D. Pritchard, C. S. Adams, and K. J. Weatherill, ARC: An open-source library for calculating properties of alkali Rydberg atoms, Comput. Phys. Comm. **220**, 319 (2017).

[88] K. Gillen-Christandl, G. D. Gillen, M. J. Piotrowicz, and M. Saffman, Comparison of Gaussian and super Gaussian laser beams for addressing atomic qubits, Appl. Phys. B **122**, 131 (2016).

[89] C. Rigetti, J. M. Gambetta, S. Poletto, B. L. T. Plourde, J. M. Chow, A. D. Córcoles, J. A. Smolin, S. T. Merkel, J. R. Rozen, G. A. Keefe, M. B. Rothwell, M. B. Ketchen, and M. Steffen, Superconducting qubit in a waveguide cavity with a coherence time approaching 0.1 ms, Phys. Rev. B **86**, 100506(R) (2012).